JOURNAL OF GEOPHYSICAL RESEARCH, VOL. 102, NO. C1, PAGES 1011-1025, JANUARY 15, 1997

# Seasonal variation of the three-dimensional mean circulation over the Scotian Shelf

Guoqi Han
Fisheries and Oceans Canada, Bedford Institute of Oceanography, Dartmouth, Nova Scotia Canada

Charles G. Hannah
Oceadyne Environmental Consultants, Bedford, Nova Scotia, Canada

John W. Loder and Peter C. Smith
Fisheries and Oceans Canada, Bedford Institute of Oceanography, Dartmouth, Nova Scotia Canada

**Abstract.** The seasonal-mean circulation over the Scotian Shelf is studied numerically by computing mean and tidal current fields for winter, spring, and summer using a three-dimensional nonlinear diagnostic model. The mean current fields are forced by seasonal-mean baroclinic pressure gradients, tidal rectification, uniform wind stresses, and associated barotropic pressure gradients. A historical hydrographic database is used to determine the climatological mean baroclinic forcing. Upstream open boundary conditions are estimated from the density fields to give no normal geostrophic bottom flow and are specified as either along-boundary elevation gradients or depth-integrated normal velocities. The numerical solutions for nominal bimonthly periods (January-February, April-May, and July-August) reveal the dominant southwestward nearshore and shelf-break flows of relatively cool and fresh shelf water from the Gulf of St. Lawrence and Newfoundland Shelf, with speeds up to about 20 cm/s. The seasonal intensification of the southwestward flows is reproduced by the model, with the transport increasing from 0.3 Sv in summer to 0.9 Sv in winter on the inner Halifax section. There are also pronounced topographic-scale influences of submarine banks, basins, and cross-shelf channels on the circulation, such as anticyclonic gyres over banks and cyclonic gyres over basins. Baroclinicity is the dominant forcing throughout the domain, but tidal rectification is comparable on the southwestern Scotian Shelf (e.g., about 0.2 Sv recirculating transport around Browns Bank for all the periods). The mean wind stress generates offshore surface drift in winter. The solutions are in approximate agreement with observed currents and transports over the Scotian Shelf, although there are local discrepancies.

## 1. Introduction

The Scotian Shelf off Nova Scotia (Figure 1), bounded by Laurentian Channel to the east and Northeast Channel to the west, is 700 km long and 160-240 km wide with an average depth of about 90 m. The highly irregular bottom relief is characterized by deep basins at midshelf (e.g., Emerald Basin) and shallow outer banks (e.g., Browns Bank). Water mass structure in this region is controlled primarily by (1) seasonally varying air-sea interaction, (2) the confluence of the Cabot Strait outflow from the Gulf of St. Lawrence with the Labrador Current from the Newfoundland Shelf and offshore Slope Water, and (3) tidal mixing in the Gulf of Maine. Therefore significant spatial and temporal variations in the regional circulation are expected. Knowledge of the mean circulation and seasonal variability on the Scotian Shelf has been gained from many sources, such as water mass analysis [*McLellan*, 1954], drift bottle studies [*Trites and Banks*, 1958], geostrophic and steric calculations [*Sutcliffe et al.*, 1976; *El Sabh*, 1977; *Drinkwater et al.*, 1979; *Csanady*, 1979], moored current measurements [*Smith et al.*, 1978; *Smith and Petrie*, 1982; *Smith*, 1983; *Anderson and Smith*, 1989; *Smith*, 1989], satellite altimetry [*Han et al.*, 1993], and numerical models [*Greenberg*, 1983; *Wright et al.*, 1986; *Tee et al.*, 1993]. Collectively, these studies have revealed the dominant circulation pattern [*Smith and Schwing*,



Paper number 96JC03285.
0148-0227/97/96JC-03285$09.00

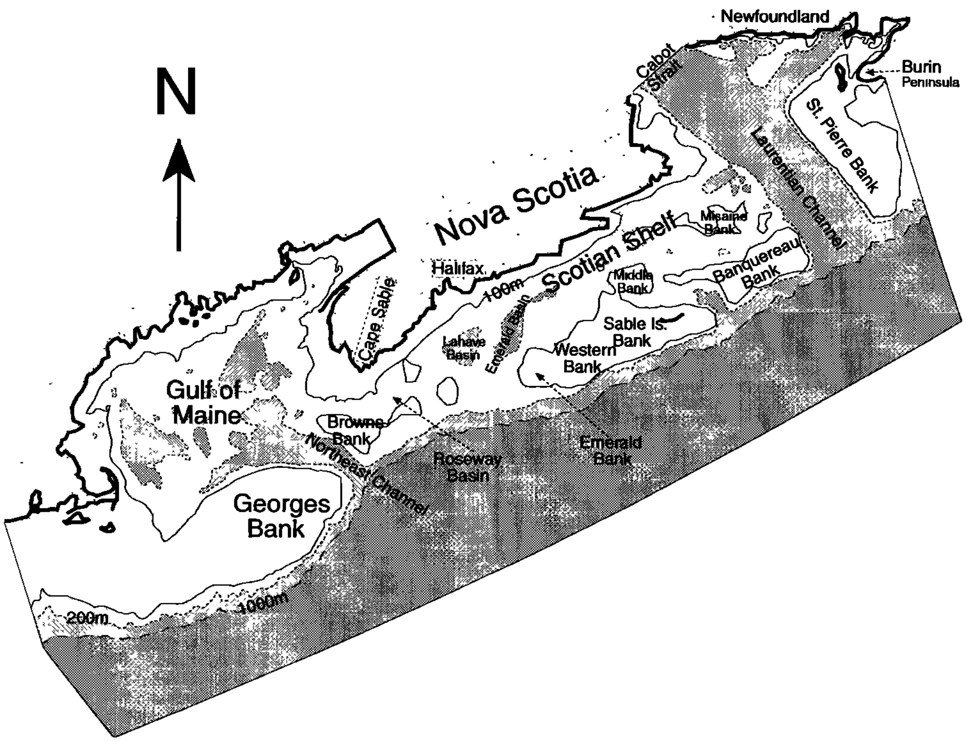


**Figure 1.** Map showing bathymetry and feature locations in the computational domain extending from the southern Newfoundland Shelf to the Middle Atlantic Bight. The isobaths shown are 100, 200, and 1000 m.

1991], namely southwestward flows with strong seasonal variability in both nearshore and shelf-break regions, and some prominent local features, such as strong tidal rectification off southwestern Nova Scotia.

In recent years, increased availability of historical temperature-salinity data together with three-dimensional (3-D) diagnostic circulation models have provided improved quantitative descriptions of the seasonal-mean hydrography and baroclinic circulation on the Scotian Shelf [*Hannah et al.*, 1996; *Loder et al.*, 1996; *Sheng and Thompson*, 1996]. In particular, *Hannah et al.* [1996] and *Loder et al.* [1996] have used climatological seasonal-mean density fields and a linear finite-element model [*Lynch et al.*, 1992] to show that the seasonally varying baroclinic circulation is generally the dominant component of the seasonal-mean circulation in the Scotian Shelf and Gulf of Maine region. More detailed studies on Georges Bank [*Naimie et al.*, 1994] (hereafter NLL94) [*Naimie*, 1996] and in the Gulf of Maine [*Lynch et al.*, 1996] with additional forcings and more sophisticated models have confirmed the importance of the baroclinic circulation in these areas.

In this paper, we use the 3-D nonlinear diagnostic circulation model of NLL94 to examine the climatological seasonal-mean circulation on the Scotian Shelf associated with the combined influences of seasonally varying baroclinicity, $M_2$ tidal rectification, and wind stress. Our goals are to provide a quantitative estimate of the 3-D shelf-wide circulation field, quantify the contributions of the three primary forcings, and evaluate the model current fields against available in situ observations. This study can thus be viewed as a Scotian Shelf counterpart to the NLL94 Georges Bank study and an intermediate step in the progression from diagnostic studies of the baroclinic flow component [e.g., *Hannah et al.*, 1996] to planned prognostic model applications to the Scotian Shelf.

Section 2 contains brief descriptions of the finite-element circulation model, the procedure for estimating density fields and other forcings, and the database of moored current measurements. The circulation model results are presented in section 3, where the model flow fields for three seasons (winter, spring, and summer) are described, interpreted, and compared with the in situ observations. The sensitivity of the circulation to several model parameters is discussed in section 4, and section 5 summarizes the results.

## 2. Methodology

### 2.1. Circulation Model

The 3-D circulation associated with the baroclinic pressure fields, upstream boundary flows, tidal rectification, and surface wind stress is examined using FUNDY5IT, a version of the nonlinear diagnostic model used in NLL94. The model consists of the nonlinear 3-D shallow water equations with hydrostatic and Boussinesq assumptions and a vertical eddy viscosity closure. As described by NLL94, the eddy viscosity has a quadratic dependence on the vertically averaged velocity, depends on the vertically varying gradient Richardson number to account for the effects of stratification, and includes a background value of 0.002 $m^2/s$ to represent the influence of unmodeled currents (with an assumed depth-averaged speed of 0.1 m/s). The model has a quadratic bottom stress law applied at about 1 m above the actual seafloor, with an additional linear term to account approximately for the influence of unmodeled currents (with an assumed average near-bottom speed of 0.07 m/s), again as given by NLL94. The model's horizontal grid points are the nodes of a triangular finite-element mesh extending along shelf from the Burin Peninsula (Newfoundland) to Long Island (New York) (Figure 1; also see Figure 2 of *Loder et al.* [1996]). The mesh has 8949 nodes, with realistic bottom topography shoreward of the 1000-m isobath, and a false bottom in the deep ocean which slopes gently to 1200 m at the offshore boundary. The model's vertical mesh has 21 unequally spaced nodes that lie approximately on constant $\sigma(= z/h)$ levels (where $z$ is the vertical coordinate and $h$ is the local water depth), with minimum spacing of 2.5 m at the surface and bottom.

The model uses a two-frequency harmonic method to solve iteratively the nonlinear 3-D shallow-water equations [*Lynch and Naimie*, 1993; *Naimie and Lynch*, 1993] (NLL94). The vertically averaged governing equations are solved for the free surface elevation, followed by a vertical computation for the horizontal velocities and solution of the three-dimensional continuity equation for the vertical velocities. The baroclinic pressure gradients on the model's vertical mesh are obtained from vertical interpolation of the pressure gradients computed on the level surfaces of the optimal interpolation grid (next subsection).

Forcing is included from the baroclinic pressure gradient computed from climatological seasonal-mean density fields (next subsection), the $M_2$ tide, and surface wind stresses (section 2.3). Boundary conditions for the mean circulation include no normal depth-integrated flow on the land and truncated Bay of Fundy boundaries, and a geostrophic-flow condition on the downstream cross-shelf boundary. For each season, a solution is obtained with steric conditions (estimated from the density field to give no geostrophic flow normal to the boundary at the seafloor) specified on the Cabot Strait (CS), southern Newfoundland Shelf (SNS), and offshore boundaries. Wind-forced contributions to the upstream boundary flows are neglected, since their influence on the seasonal-mean currents on the Scotian Shelf is estimated to be relatively small, based on the studies of *Schwing* [1992a b] and D. A. Greenberg et al. (Spatial and temporal structure of the barotropic response of the Scotian Shelf and Gulf of Maine to surface wind stress: A model-based study, submitted to *Journal of Geophysical Research*, 1996)(hereafter referred to as Greenberg et al., submitted manuscript, 1996). Other barotropic flows of upstream origin are also neglected, in order to evaluate the extent to which local and baroclinic boundary forcings alone can account for the observed circulation. The steric conditions are in the form of specified elevations on the SNS and offshore boundaries and of the corresponding depth-averaged normal velocity on the CS boundary (in order to allow natural adjustment of the mean elevation on this boundary). At the $M_2$ tidal frequency, elevations are specified at the open boundaries, as described in section 2.3.

## 2.2. Density Fields

Climatological seasonal-mean density fields for winter, spring, and summer were estimated from the Bedford Institute's hydrographic database using four-dimensional optimal linear interpolation [*Bretherton et al.*, 1976]. This procedure provides estimates of the mean fields at specified grid points in four-dimensional space ($x$,$y$,$z$,$t$), from their nearest-neighbor data based on separation distances scaled by specified correlation scales in an assumed covariance function (see *Loder et al.* [1996] for more detail on the database and interpolation procedure).

Briefly, the hydrographic database comprises about 54,000 stations with coincident temperature and salinity observations and positions distributed across (and slightly beyond) the model domain (Figure 1), with poorest coverage generally in winter and in eastern and offshore areas. In the Scotian Shelf portion of the domain, the database has approximately 4900, 7400, and 9800 stations (profiles extending more than 20 m below the surface) in winter, spring, and summer, respectively. After standard quality control and subsampling of the conductivity-temperature-depth (CTD) data, density fields were estimated at the horizontal grid points of the finite-element mesh, at level surfaces in the vertical, and at seasonal midtimes (February 1, May 1, and August 1 for winter, spring, and summer, respectively). The fields were also estimated at levels below the seafloor, so that the horizontal density and baroclinic pressure gradients could be computed on level surfaces, and then vertically interpolated to the model's vertical mesh.

The correlation (roughly, e-folding) scales in the optimal interpolation procedure were specified following the approach of *Loder et al.* [1996] which approximates expected spatial structure (e.g., due to topography) in the shelf hydrography and provides smoothed fields in the data-sparse slope and deep-ocean regions. Temporal correlation scales of 60 days, larger than those given by *Loder et al.* so as to provide increased temporal averaging in data-sparse areas, were used for the three periods. Sensitivity of the baroclinic circulation to this choice will be discussed in section 4. The spatial correlation scales were specified as in the base case given by *Loder et al.* (see their Appendix), with horizontal (topo-

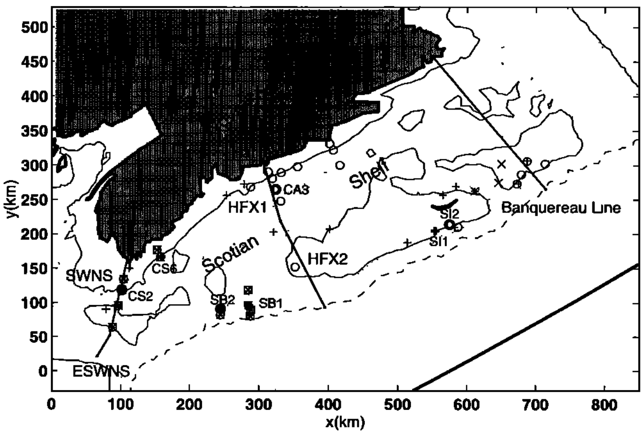


**Figure 2.** Map showing bathymetry (100-, 200-, and 1000-m isobaths), cross-shelf sections, and current meter mooring sites over the Scotian Shelf. The model origin is at 42N, 67W. The thick solid lines labeled HFX1, HFX2, and SWNS indicate the locations of vertical sections used for Tables 1, 3, and 4. The Banquereau line and Halifax (HFX1+HFX2) and extended SWNS (ESWNS) sections are used in Figures 4, 7, and 11. Open circles, crosses, and plusses indicate the locations of current meter mooring sites for winter, spring and summer, respectively. Detailed current comparisons are presented in Figure 9 for the labeled sites (thick circles and plusses).

graphic) anisotropy in the horizontal correlation scales over the shelf and slope specified through parametric relationships involving the local water depth and bathymetric gradient vector. The parameterization assumes isotropic scales of 40, 40, and 30 km for uniform-depth shelf areas in winter, spring and summer, respectively, and provides increased scales in the along-isobath direction and decreased scales in the cross-isobath direction over sloping topography, qualitatively consistent with observed patterns (e.g., sea surface temperature from satellite imagery). The along-isobath scales increase to 100-200 km over the upper continental slope and then increase further to approximate the deep-ocean along-shelf (65°T) scale of 400 km. In contrast, the cross-isobath scales decrease to 15-20 km over the upper slope and then increase again to approximate the deep-ocean cross-shelf scale of 60 km. An additional anisotropy was introduced in Laurentian Channel ($h > 200$ m), providing along- and cross-channel scales of 150 and 15 km, respectively, to reflect the channel geometry in areas of weak bottom slope. Finally, the vertical correlation scales were specified to increase with depth below the surface, ranging from 15 m in the upper 60 m to 200 m at 1200-m depth. The uncertainty in the computed density fields is estimated to be of order 0.1 $\sigma_t$ units, with largest values in offshore and eastern areas and near the seafloor and smallest values on the western and central Scotian Shelf.

Three cross-shelf sections (Figure 2) are used to illustrate the spatial and temporal structure of the resulting density fields on the Scotian Shelf: the Banquereau line, a Halifax section, and an extended southwestern Nova Scotia (ESWNS) section. Figure 3 presents the vertical density distributions for winter and summer along these sections, and Figure 4 presents the horizontal dis-

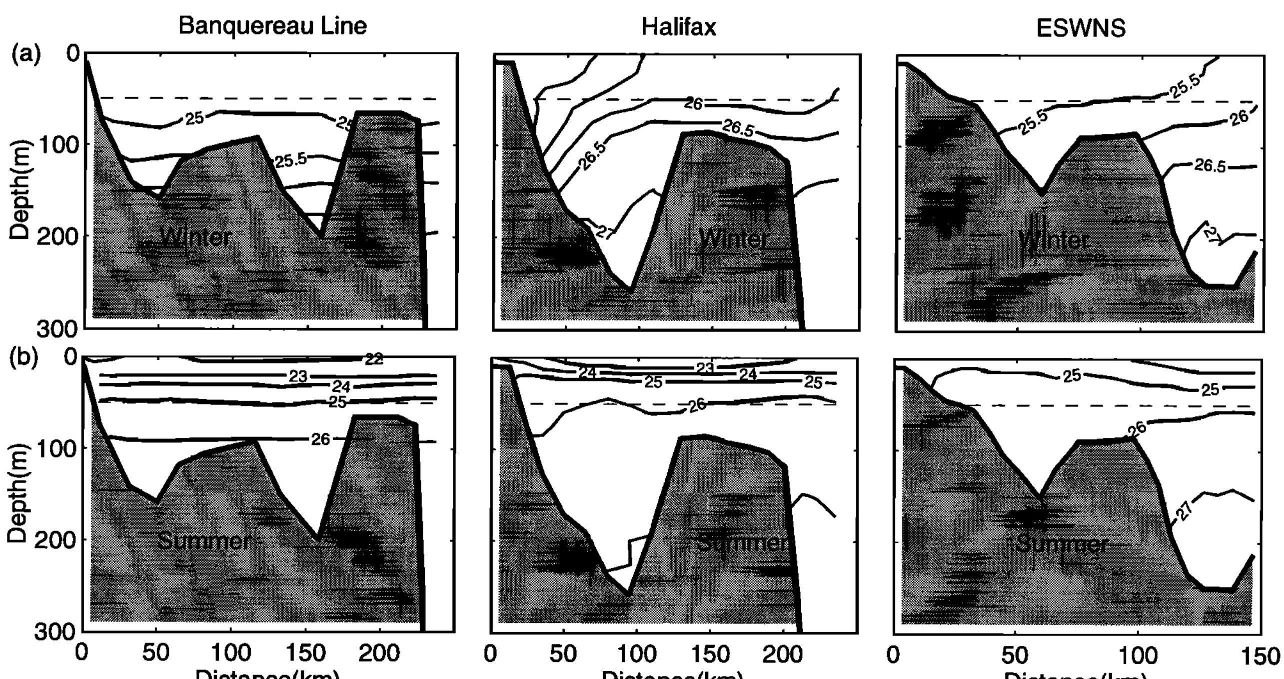


**Figure 3.** Vertical distribution of density ($\sigma_t$ units) on the Banquereau line, and Halifax and ESWNS sections computed from the historical database for (a) winter and (b) summer. The contour interval is 0.5 $\sigma_t$ in Figure 3a and 1.0 $\sigma_t$ in Figure 3b, and the dashed line is the 50-m level.

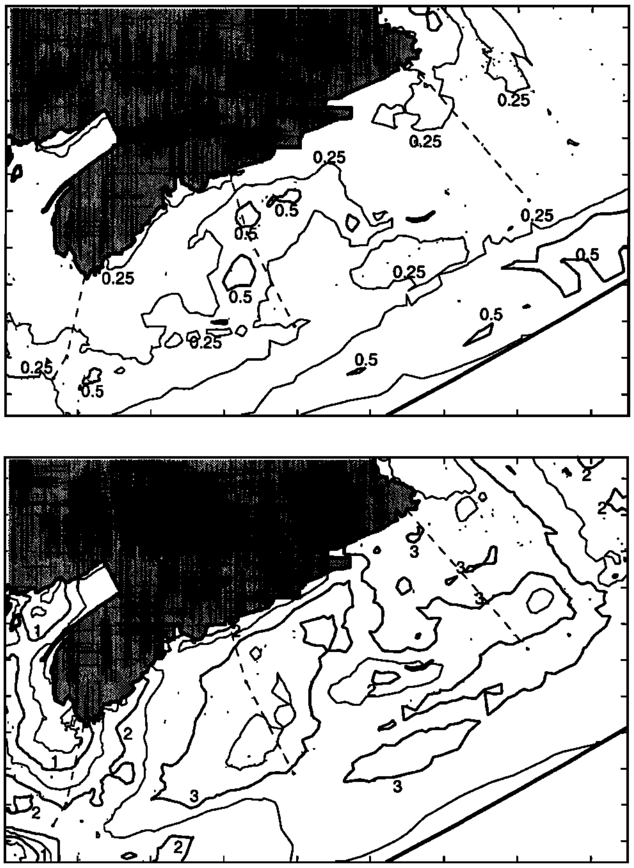


**Figure 4.** Areal distribution of the density difference ($\sigma_t$ units) between 50 m (or the bottom for water depth < 50 m) and the surface for (a) winter and (b) summer. The contour interval is 0.25 $\sigma_t$ in Figure 4a and 0.5 $\sigma_t$ in Figure 4b, and the dashed lines indicate the locations of the sections in Figure 3.

tributions of the density difference between 50 m (or the bottom for water depth < 50 m) and the surface. The density structure in winter (Figures 3a and 4a) shows generally weak stratification in the upper 50 m, with strongest stratification at depth in basins and channels, and over the continental slope. On the Halifax section, there is strong geostrophic shear (sloping isopycnals) on the inner shelf, associated with the seasonal maximum in the Nova Scotia Current. In summer (Figures 3b and 4b), strong stratification is well developed over most of the shelf and concentrated in the near-surface layer, with density differences of more than 3.0 $\sigma_t$ units over Emerald Basin. Exceptions to this are the year-round vertically mixed areas off southwestern Nova Scotia and on Georges Bank where there are local tidal-mixing fronts. Summertime along-shelf gradients in both surface density (Figure 3b) and stratification (Figure 4b) are clearly apparent. The density field for spring (not shown) is an intermediate step in the seasonal evolution between winter and summer. Refer to *Loder et al.* [1996] for discussion of the associated temperature and salinity distributions and *Hannah et al.* [1996] for discussion of the associated steric height and potential energy distributions.

### 2.3. Other Forcings

The mean wind stresses for the bimonthly periods and the $M_2$ tidal elevations on open boundaries are also used as model input. The wind stresses were based on hourly wind measurements from Sable Island on the eastern Scotian Shelf (Figure 1) for 1953 to 1986, compiled at the Bedford Institute of Oceanography (R. Lively, personal communication, 1995). Sable Island stresses are approximately representative of monthly and lower-frequency stresses over much of the Scotian Shelf [*Smith*, 1987]. Stresses were computed using a quadratic friction law with the neutral-stability speed-dependent drag coefficients of *Smith* [1988]. The resulting climatological means for the present bimonthly seasons (Figure 5) show a strong seasonal variation in both magnitude and direction, with the winter stress being stronger and directed more cross shelf (offshore) than the spring and summer stresses.

The $M_2$ tidal elevations on most of the open boundaries (those west of Laurentian Channel and Cabot Strait) are the same as those used by Greenberg et al. (submitted manuscript, 1996) in obtaining friction coefficients from a nonlinear barotropic tidal solution with the *Lynch and Naimie* [1993] iterative model. The elevations on the other open boundaries are taken from *de Margerie and Lank* [1986] and *Han et al.* [1996]. The $M_2$ constituent generally dominates tidal current variability over the Scotian Shelf, except for the eastern portion where the $K_1$ current is also important.

### 2.4. Moored Current Meter Data

Our primary source of observed mean currents is a database of monthly current statistics from moored measurements on the Scotian Shelf [*Gregory and Smith*, 1988]. We chose 29, 15, and 27 horizontal sites (Figure 2) in winter, spring, and summer, respectively, for comparison of the moored current meter data with the model solutions. Most of these mooring sites were chosen from the Canadian Atlantic Storms Program (CASP) [*Anderson and Smith*, 1989], the Shelf Break Experiment [*Smith and Petrie*, 1982], and the Cape Sable Experiment [*Smith*, 1983] to represent the dominant alongshore coastal and shelf-break currents over the Scotian Shelf and the tidally rectified gyre circulation over Browns Bank. Monthly means for a particular instrument/depth are included for each month with at least 20 days of data. Typically, each site has data from two or three depths in 1 or 2 years, resulting in 79, 39, and 68 different 3-D positions in winter, spring, and summer, respectively. For comparison with the model flow fields, bimonthly mean currents and standard deviations have been computed for each vertical level by averaging over all months and years in each bimonthly season.

The major features of the observed seasonal-mean residual circulation on the Scotian Shelf are apparent in the bimonthly mean current distributions (Figure 5) for the upper (within 20 m of surface) and lower layers. The currents are generally directed southwestward on the shelf throughout the year but demonstrate strong seasonal, horizontal, and vertical variations in magnitude. The currents are generally strongest in the winter, in the near-surface layer, and in the vicinity of the nearshore 100-m isobath and the shelf break. The clockwise topographic-scale circulation over Browns Bank is persistent throughout the year, with some increase in summer. There are also more complex current patterns in some areas, such as the Sable Island region in summer, probably reflecting aliased temporal as well as actual spatial variability.

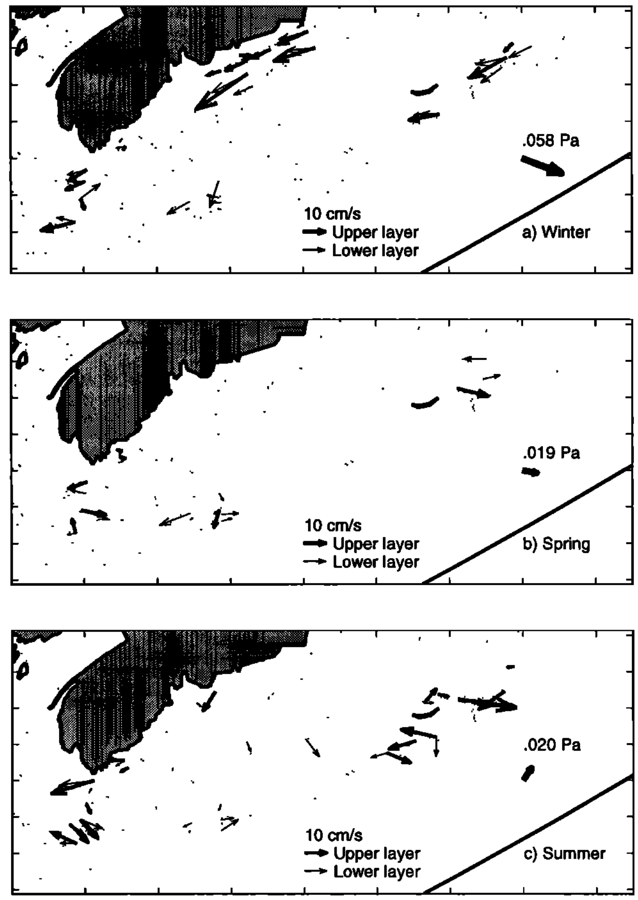


**Figure 5.** Bimonthly mean currents from moored measurements for upper layer (within 20 m of surface) and lower layer (remainder of the water column) regions, computed by vertical averaging for (a) winter, (b) spring, and (c) summer. The bimonthly mean wind stresses at Sable Island are shown by the thickest arrows on the right. The 100-, 200- and 1000-m isobaths are displayed for reference.

## 3. Bimonthly Circulation Fields

### 3.1. Overview

In this section we present model results for the seasonal-mean circulation forced by the mean density fields and associated steric boundary conditions, the $M_2$ tide, and the mean wind stresses.

The transport stream functions (Figure 6) for the bimonthly solutions indicate both persistent features and strong seasonal variation. Vertical and horizontal sections of the (Eulerian) mean circulation are presented in Figures 7 and 8. For all periods the dominant features are southwestward flow nearshore and over the shelf break and northeastward flow further offshore. The shelf and shelf-break currents are associated with outflow through Cabot Strait from the Gulf of St. Lawrence and extension of the Labrador Current from the Newfoundland Shelf. Smaller-scale eddy-like features are apparent in areas with strong topographic variability such as banks, basins, and the shelf break; while most of these features appear to be realistic, some are probably artifacts of local density structures arising from data sparsity and/or aliasing of temporal variability (e.g., at the shelf break on the western Scotian Shelf). Comparison of the mean transports at the selected sections (Table 1) and the mean velocities at the mooring sites (Figure 9 and Table 2) with the observational data presented in section 2 indicates modest quantitative agreement, although there are significant discrepancies both locally and overall in some seasons. A more detailed description of the bimonthly circulation fields and their comparison with observations is presented in the following three subsections.

We also present (Table 3) estimates of the individual contributions for the three primary forcings: tidal rectification (including stratification influences on friction), baroclinic pressure gradients and associated steric flows at the upstream boundaries, and wind stress, following the approach of NLL94.

### 3.2. Winter Season: January-February

In the winter season, when the southwestward shelf currents are most intense (e.g., Table 1), the depth-integrated stream function pattern (Figure 6a) clearly shows the dominant southwestward flows along both the Nova Scotian coast and the shelf break. The major contributor to the shelf-break flow is the extension of the Labrador Current from the southern Newfoundland Shelf, while the nearshore branch (the Nova Scotian Current) is fed by both the extension of the Labrador Current and the outflow from the Gulf of St. Lawrence (note, however, that the reliability of the elongated anticyclonic cell over Laurentian Channel is unclear; also see *Loder et al.* [1996]). There is a weak northeastward counterflow between the Nova Scotian Current and the coast (Figure 7a), which was clearly observed at station 1 during CASP [*Anderson and Smith*, 1989] and explained by *Smith and Schwing* [1991]. A weak branch

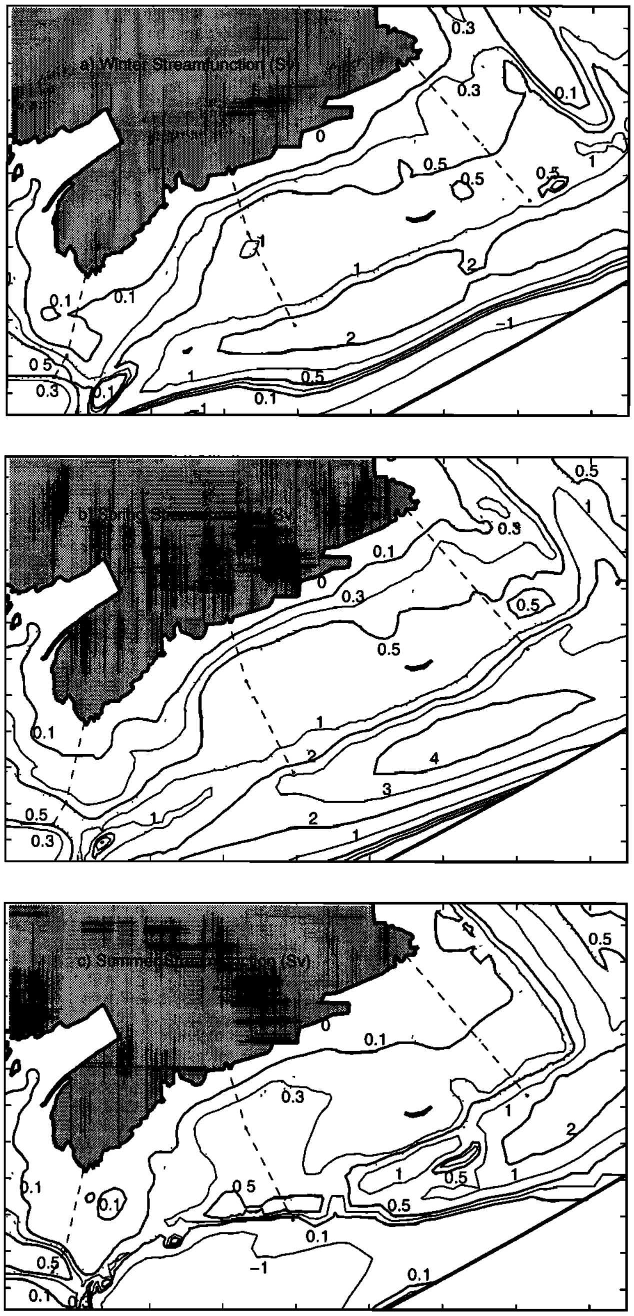

**Figure 6.** Transport stream function for (a) winter, (b) spring, and (c) summer from model solutions with full forcing. The flow is cyclonic around positive stream function extrema and anticyclonic around negative stream function extrema. The stream function is zero at the coast so that offshore values at particular positions indicate the integrated transport between these positions and the coast. The 200-m isobath (dotted lines) and the cross-shelf sections (dashed lines) are included.

of the shelf-break current turns clockwise around Western Bank (Figure 8a) and then westward as part of a cyclonic gyre around Emerald Basin and finally merges again with the strong branch which follows the shelf break. West of the Halifax section, a large portion of the nearshore current is directed offshore to join the shelf-break current on the southeastern flank of Browns Bank, which then feeds the inflow on the eastern side of Northeast Channel. A similar surface circulation pattern to Figure 8a over the eastern and central Scotian Shelf was obtained from vertical density profiles alone [*Sheng and Thompson*, 1996], suggesting that baroclinic circulation dominates. An anticyclonic gyre is evident over the western cap of Browns Bank (Figure 8a), while to the northeast, there is a weaker cyclonic gyre over Roseway Basin. Over the shelf break and offshore, an equatorward transport in excess of 1 Sv reaches the western Scotian Shelf before turning offshore (also see *Hannah et al.*, 1996). This pattern is consistent with the cyclonic Slope Water gyre described in previous studies [e.g., *Csanady and Hamilton*, 1988].

The model velocity distribution on the Banquereau line (Figure 7a) shows a southwestward inner-shelf current with peak speed near 20 cm/s at the surface and a shelf-break current with peak (surface) speed near 15 cm/s. The model currents on the Halifax section are dominated by southwestward flow in both the shelf-break jet and the Nova Scotian Current on the inner shelf, both with maximum speeds of over 20 cm/s near the surface. However, there is a weak northeastward current (up to 5 cm/s) on the northern flank of Emerald Bank associated with the current branch that meanders onto the shelf. On the ESWNS section, the dominant transport feature is a northwestward jet with a maximum velocity of about 15 cm/s on the southwestern flank of Browns Bank. The vertical extent of this feature suggests that it includes both Scotian Shelf and Slope Water [e.g., *Brown and Beardsley*, 1978; *Ramp et al.*, 1985] although the flow pattern offshore of Northeast Channel is confounded by a suspect eddy (Figure 6a). On the northern flank of Browns Bank, there is a narrow (10 km) eastward flow of 5-10 cm/s over entire water column caused by tidal rectification and amplified by reductions in the vertical eddy viscosity due to stratification. Other features associated with tidal rectification include a nearshore westward jet with a maximum velocity of 10 cm/s and near-bottom upwelling off Cape Sable, consistent with *Tee et al.'s* [1993] finding. Even though this season has the strongest wind stress, its influence is limited and largely confined to the near-surface (upper 10 m) layer (e.g., Figure 9a), in part because it is directed more cross shelf than along shelf (e.g., Greenberg et al., submitted manuscript, 1996). We shall not attempt to interpret further the cross-shelf velocity component on the sections since its character is sensitive to the choice of coordinate system.

The local current comparison (Table 2) indicates that the model flow fields for the winter season show approximate quantitative agreement with observations, with the average magnitude of currents in the model being about 90% of that observed. There are, however, no-

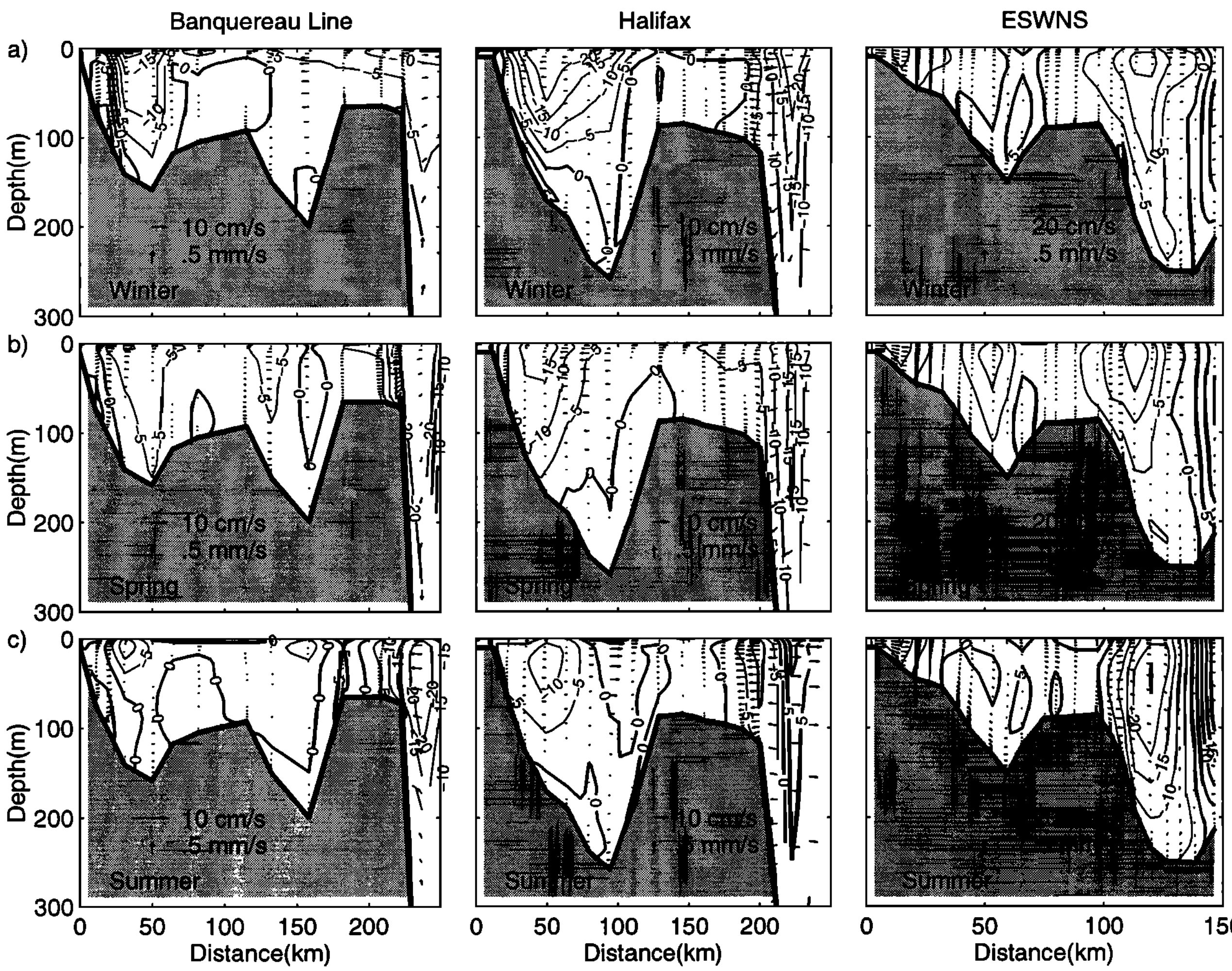


**Figure 7.** Mean velocity on the Banquereau line and the Halifax and ESWNS sections for (a) winter, (b) spring, and (c) summer from model solutions with full forcing. Isotachs (centimeters per second) of the normal component (positive into the page) and vector representations of the tangential component are shown. The isotach interval is 5 cm/s, with positive (and zero) isotachs in thick lines and negative ones in thin lines.

table discrepancies, with the average magnitude of the vector velocity difference between model and observations nearly 60% of the observed average magnitude, and an average difference angle of 33°. The detailed comparison at selected mooring sites (Figure 9a) indicates approximate agreement for the vertical shear in most cases and good quantitative agreement for the currents at sites SB2, SI2, and CA3. However, the observed westward flow at site CS2, the site with the largest moored measurement data set, is underpredicted (also see section 4.2).

Comparison of the winter transports (Table 1) with moored measurements on the HFX1 (1.0 Sv [*Anderson and Smith*, 1989]) and southwestern Nova Scotia (SWNS) (0.32 Sv [*Smith*, 1983]) sections indicates good agreement. This suggests that the overall shelf flow patterns are generally robust and realistic. It appears that to the level of observational accuracy, additional barotropic flow over most of the shelf (through specification of barotropic inflow on the upstream boundary) is not required. However, additional barotropic flow over the slope region cannot be ruled out, in view of model approximations, data sparsity and the limited current comparisons. The present results, supported by moored measurements [*Anderson and Smith*, 1989], also suggest that the geostrophic transport through the HFX1 section in winter was underestimated at about 0.44 Sv by *Drinkwater et al.* [1979] due to their assumed 100-m level of no motion (see the deeper level of no motion in Figure 7a and at CA3 of Figure 9a).

The transport estimates for the three processes (Table 3) indicate that baroclinic circulation controls the southwestward flow on the Scotian Shelf in the winter season, even though wind stress and tidal rectification make important contributions on the southwestern Scotian Shelf. The small net contribution from tidal rectification results from offsetting flows on the flanks of Browns Bank, with the tidally rectified recirculating

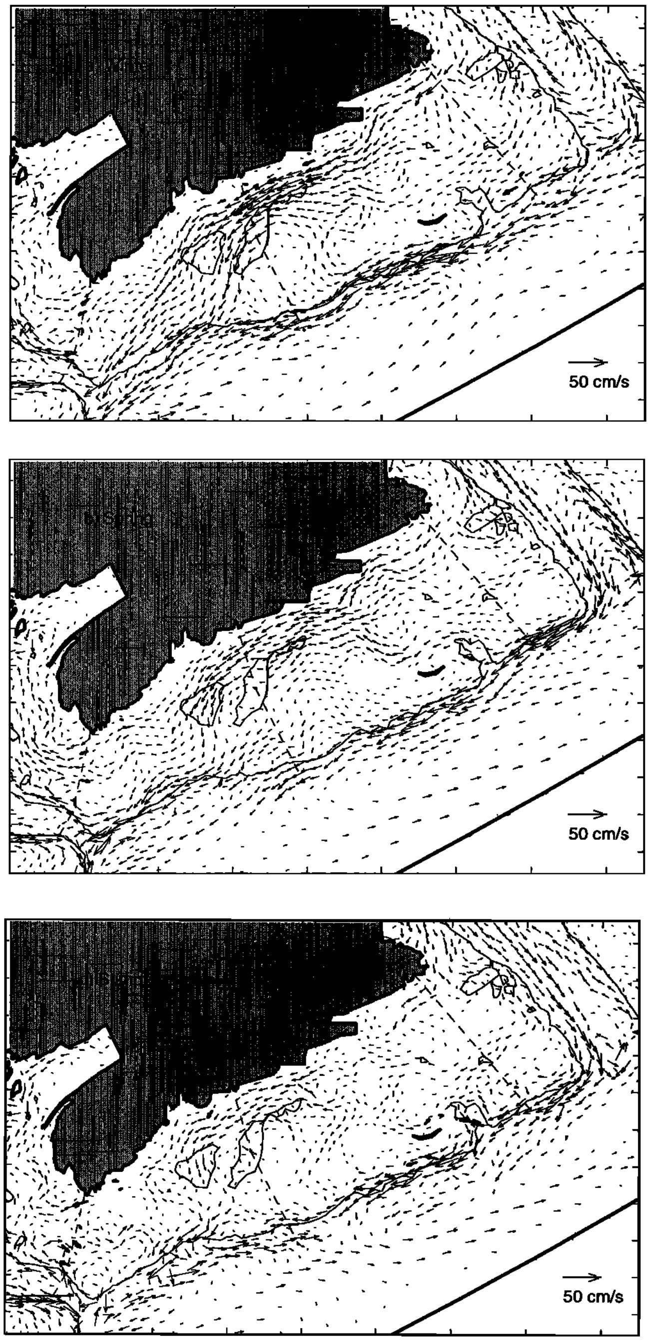


**Figure 8.** Near-surface (averages between 5 and 25 m of the surface) mean currents (thin arrows) for (a) winter, (b) spring, and (c) summer from model solutions with full forcing. The modeled vector fields have been subsampled for presentation. The observed near-surface (within 20 m of surface) currents (thick arrows) are also shown (taken from Figure 5). The 200-m isobath (solid curve) and cross-shelf sections (dashed lines) are included.

transport around Browns Bank amounting to 0.19 Sv. These results are consistent with previous studies pointing to the general dominance of the baroclinic circulation [*Hannah et al.*, 1996; *Sheng and Thompson*, 1996] and the increased importance of wind stress (Greenberg et al., submitted manuscript, 1996) and tidal rectification [e.g., *Greenberg*, 1983] off southwestern Nova Scotia. It is also important to mention that the section transport estimates in Tables 1 and 3 are sensitive to the offshore extent of the sections since the latter cross recirculating gyres. Here the offshore positions approximate those used by *Smith* [1983] for the SWNS section, and by *Anderson and Smith* [1989] and *Drinkwater et al.* [1979] (from the coast to their station 3) for the HFX1 section.

**Table 1.** Comparison of Transports Across Selected Sections (Figure 2) in the Model Solutions Under Full Forcing, with Observational Estimates

| Period | HFX1 | | SWNS | |
|---|---|---|---|---|
| | Modeled | Observed | Modeled | Observed |
| Jan.-Feb. | 0.92 | 1.0 | 0.25 | 0.32 |
| April-May | 0.81 | ... | 0.51 | 0.19 |
| July-Aug. | 0.41 | 0.25 | 0.15 | 0.03 |

Units are Sverdrups. Estimates are from *Smith* [1983], *Anderson and Smith* [1989], and B. Petrie (personal communication, 1996). Postive transports are along shelf towards the southwest. (Observational transports are not available for the Banquereau line).

### 3.3. Summer Season: July-August

The summer model solution shows generally weakened flow on the shelf (Figures 6c, 7c, and 8c). One difference from the winter solution is that the outflow from the Gulf of St. Lawrence has a major pathway along the western side of Laurentian Channel, merging with the extended Labrador Current over the slope (Figure 6c). Another difference is reduced circulation over Emerald Basin (Figure 8c). Over the continental slope off the western Scotian Shelf, the northeastward slope current reaches the shelf break (Figure 6c), possibly due to weaker upstream inflow as suggested by weaker observed shelf-break currents (Figure 5c). While this northward seasonal excursion of the Slope Water influence is qualitatively consistent with *Drinkwater et al.'s* [1994] analysis of shelf/slope frontal position, an excursion of the magnitude implied by the present winter and summer circulation patterns (Figures 6a and 6c) is not apparent in the associated salinity fields (e.g., Figure 5 of *Loder et al.* [1996]) nor in *Drinkwater et al.'s* analysis. This raises questions as to the reliability of the slope circulation off the western Scotian Shelf in the summer solution (also see section 4.1).

Compared with the winter solution, the southwestward inner-shelf flow on the Banquereau line is weakened, while the southwestward shelf-break current is intensified but narrowed (Figure 7c). Another difference in the summer solution is a northeastward flow on the northern flank of Banquereau Bank, as part of an an-

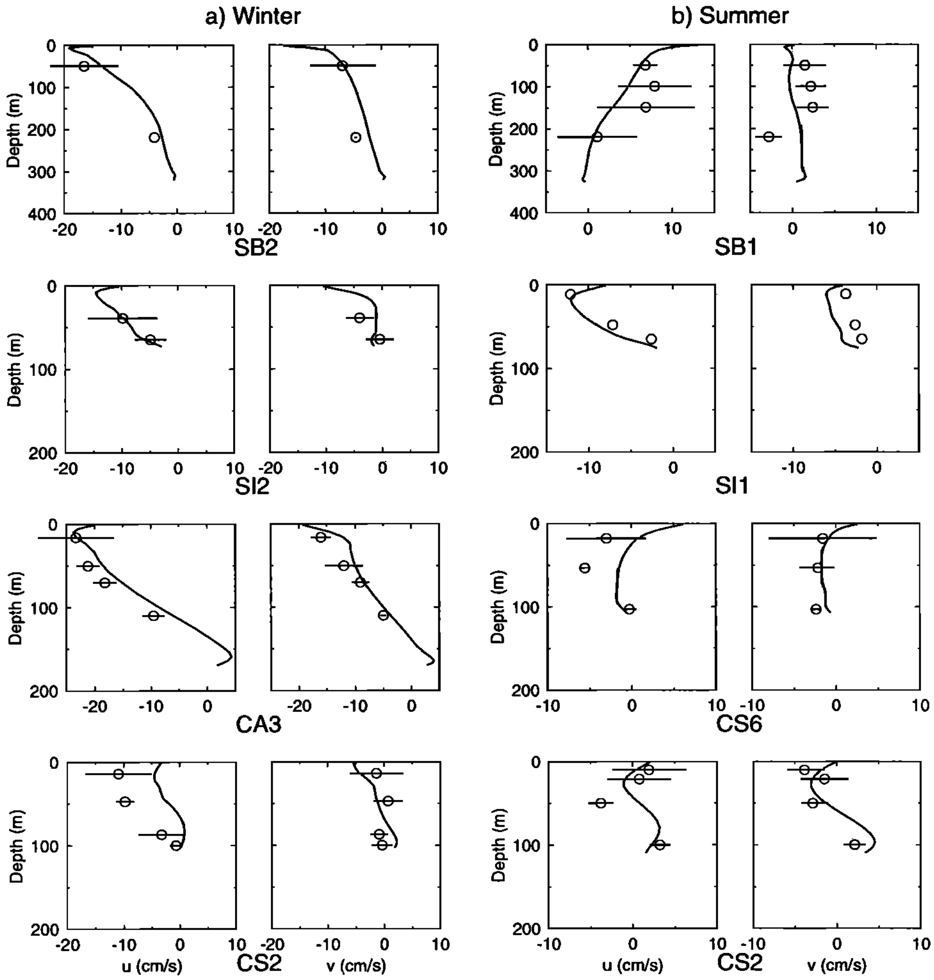


**Figure 9.** Comparison of current profiles from the model solutions under full forcing (solid curves) with observed bimonthly mean currents (open circles) for (a) winter and (b) summer. Here $u$ and $v$ are the eastward and northward components, respectively. The horizontal lines indicate the standard deviations of the individual observed monthly means about the bimonthly means. The site locations are shown in Figure 2.

ticyclonic gyre over the bank (see Figure 8c). On the Halifax section, both the inshore and shelf-break jets are weakened and significantly narrowed, with maximum speeds near 10 cm/s. The shelf-break jet is shifted shoreward and there is now a northeastward current jet over the slope. The northeastward current on the northern side of Emerald Bank is weaker and narrower, consistent with the reduced circulation around Emerald Basin. On the ESWNS section, the nearshore flow, which primarily arises from tidal rectification, is enhanced due to influences of the stronger stratification on friction (see section 4.2), with a maximum velocity

**Table 2.** Statistics (Means and Standard Deviations) of the Comparison Between Observed and Modeled Mean Currents at Moored Current Meter Positions

| Period | No. of Positions | Current Speed, cm/s | | Magnitude of VVD, cm/s | DA, degree |
|---|---|---|---|---|---|
| | | Observations | Model | | |
| Jan.-Feb. | 79 | $8.7 \pm 6.5$ | $7.7 \pm 6.4$ | $5.2 \pm 4.8$ | $33 \pm 56$ |
| April-May | 39 | $6.9 \pm 4.6$ | $5.8 \pm 3.1$ | $6.8 \pm 5.0$ | $75 \pm 71$ |
| July-Aug. | 68 | $7.5 \pm 5.5$ | $7.0 \pm 5.9$ | $6.5 \pm 4.9$ | $49 \pm 59$ |

The vector velocity difference (VVD) is the difference vector between the observed and modeled velocities at a particular site and depth. The difference angle (DA) is the difference in direction between the observed and modeled velocities.

**Table 3.** Approximate Process Partitioning of Bimonthly Transports Through Selected Sections

| Period | Processes | Transport, Sv | |
|---|---|---|---|
| | | HFX1 | SWNS |
| Jan.-Feb. | $M_2$ tidal rectification | -0.01 | 0.01 |
| | baroclinic pressure gradients | 0.92 | 0.32 |
| | wind stress | 0.01 | -0.08 |
| April-May | $M_2$ tidal rectification | -0.01 | -0.04 |
| | baroclinic pressure gradients | 0.83 | 0.60 |
| | wind stress | -0.01 | -0.05 |
| July-Aug. | $M_2$ tidal rectification | -0.01 | -0.05 |
| | baroclinic pressure gradients | 0.48 | 0.24 |
| | wind stress | -0.07 | -0.04 |

Positive transports are along shelf towards the southwest.

of 15 cm/s. The offshore jet is significantly intensified, with a maximum velocity of 25 cm/s (note that only a small fraction of this jet is included in the transport estimate in Table 1 for the SWNS section). The eastward flow reversal on the northern flank of Browns Bank has similar intensity to but is broader than that in the winter season.

The comparison of model currents with summer moored measurements (Table 2) indicates similar but slightly reduced agreement compared to the winter. Although the average magnitude of currents in the model is 93% of that observed, the deviations are greater than those in the winter, with the average magnitude of the vector difference nearly 86% of the observed average speed, and an average difference angle of 49°. At the selected mooring sites (Figure 9b), there are similarities between the model and observed profiles in all cases, but there are also significant discrepancies.

Comparison of the transports in this solution (Table 1) with the observed summer transports from moored measurements on the SWNS section (0.03 Sv [*Smith*, 1983]), and from geostrophic calculations with a moored measurement adjustment on the HFX1 section (0.25 Sv [*Drinkwater et al.*, 1979]; adjusted by B. Petrie (personal communication, 1996)), indicates approximate agreement only. Tidal rectification results in eastward flow on the northern flank of Browns Bank, offsetting the southwestward transport inshore and inside the 200-m isobath on the southern flank of Browns Bank. Note, however, that the model solution indicates an additional 0.75 Sv of northwestward transport offshore of the 200-m isobath in Northeast Channel, which was not included in *Smith's* [1983] observational estimates. While the deep portion (below 100 m) of this transport should be covered by *Ramp et al.'s* [1985] estimates for the Northeast Channel inflow (annual average of 0.26 Sv), the present solutions point to additional significant inflow of shelf water in Northeast Channel (above 100 m) that has not been included in observational estimates.

The process partitioning of the transports (Table 3) indicates that baroclinic circulation again dominates during the summer season. However, tidal rectification is also an important factor on the southwestern Scotian Shelf and the leading contributor to the eastward flow on the northern flank of Browns Bank, with the tidally rectified recirculating transport around Browns Bank reaching 0.2 Sv. The along-shelf (northeastward) summer wind stress results in a weak northeastward flow component on both sections.

### 3.4. Spring Season: April-May

The various velocity distributions in Figures 6b, 7b, and 8b indicate that the spring season is an intermediate step in the seasonal progression of the shelf circulation, but with some unique features. There is a greater baroclinic transport of the Gulf of St. Lawrence outflow onto the inner and middle Scotian Shelf than in winter and summer. Some of the outflow still moves along the western side of Laurentian Channel to the outer shelf, but the shelf-break current is mainly an extension of the Labrador Current after its excursion into Laurentian Channel (Figure 6b).

On the Banquereau line (Figure 7b), the inshore jet is in an intermediate state between its winter and summer counterpart. This season has the strongest shelf-break current on this line, but the current is narrower than in winter. On the Halifax section, the inshore jet is only slightly weaker than in the winter (Table 1), with a maximum velocity exceeding 15 cm/s, while the shelf-break jet is substantially stronger and wider than in the summer, with a maximum velocity of about 15 cm/s. Both of these jets are thus in intermediate states between their winter and summer structures. On the ESWNS section, there is increased westward flow on the inner shelf and a distinct westward jet about 55 km off Cape Sable, with a maximum velocity of over 10 cm/s. This jet is part of the southwestward flow on the inner Scotian Shelf which can be traced upstream to outflow from the Gulf of St. Lawrence (Figures 6b and 8b). The eastward flow reversal on the northern flank of Browns Bank is largely eliminated by the strong southwestward baroclinic current.

The quantitative comparison of local currents (Table 2) in the spring indicates substantially poorer agreement of the model solution with observations than in winter and summer. Although the average magnitude of currents in the model is 85% of that observed, the average magnitude of the vector differences is similar to the average observed speed, and the average difference angle is large. The reduced agreement is also apparent in the near-surface velocity comparison (Figure 8b).

Comparison of the transports in this solution (Table 1) with the observed spring transports from moored measurements on the SWNS section (0.19 Sv [*Smith*, 1983]) indicates the poorest agreement among the three seasons. The southwestward baroclinic transport greatly exceeds the tidally rectified transport reversal over

**Table 4.** Transports Across Selected Sections in the Baroclinic Solutions, Showing the Sensitivity of the Baroclinic Circulations to the Choice of the Temporal Correlation Scale

| | | Transport, Sv | |
|---|---|---|---|
| Cases | HFX1 | HFX2 | SWNS |
| Jan.-Feb. 60 day | 0.92 | 2.51 | 0.39 |
| 45 day | 0.98 | 2.64 | 0.36 |
| July-Aug. 60 day | 0.45 | -0.54 | 0.39 |
| 45 day | 0.40 | -1.54 | 0.23 |

The 45- and 30-day cases for winter and summer, respectively, are the base cases of *Loder et al.* [1996], while the 60-day cases are the present base cases. Positive transports are along shelf towards the southwest.

the northern flank of Browns Bank. The model transport on the HFX1 section is comparable to that in the winter season, which is consistent with *Han et al.'s* [1993] finding from satellite altimetry, and is much larger than *Drinkwater et al.'s* [1979] geostrophic estimate (0.23 Sv) for the upper 100 m.

The process partitioning of the transports (Table 3) indicates that baroclinic circulation dominates during the spring season all over the shelf. However, there are also significant contributions from tidal rectification (0.19 Sv recirculating transport around Browns Bank) and wind stress to the transports off southwestern Nova Scotia.

## 4. Sensitivity of Circulation

### 4.1. Sensitivity of Baroclinic Circulation to the Temporal Correlation Scale

*Loder et al.* [1996, Table 2] examined the sensitivity of baroclinic circulation to the magnitude of the bottom friction and vertical eddy viscosity coefficients, the shelf-wide topographic anisotropy in the horizontal correlation scales, additional anisotropy in the horizontal correlation scales in Laurentian Channel, and the choice of seasonal midtime in their linear diagnostic calculations. Here we examine the sensitivity of baroclinic circulation to another factor, the temporal correlation scale. In order to make the comparison straightforward and consistent with *Loder et al.'s* [1996], the linear version of FUNDY5 is used with their vertical eddy viscosity and bottom friction coefficients.

Table 4 indicates the transport sensitivity of the baroclinic solutions to the somewhat arbitrary choice of temporal correlation scales in the estimation of winter and summer mean density fields. The winter solution shows only a weak sensitivity to changes in the temporal correlation scale (Table 4), consistent with expectations for scale values much less than the annual period provided that there are sufficient density observations. The summer solution also shows only weak sensitivity over most of the domain, but significant sensitivity on the SWNS section (Table 4) and at the shelf break on the western Scotian Shelf. This sensitivity is related to the suspect northward meander (near the shelf break) of the northeastward deep-ocean flow off the western Scotian Shelf in the summer solution (Figure 6c). With the temporal correlation scale reduced to 30 days, there is increased northeastward flow at the shelf break in this region, as illustrated by the current profiles for site SB1 (Figure 10). The observed currents at this site are in much better agreement with the base (60-day) solution, suggesting that the longer temporal window provides a better representation of the local mean density field. However, this sensitivity points to the general uncertainty of the seasonal-mean circulation, both in the ocean and in models, in the complex and dynamic slope region off the western Scotian Shelf.

### 4.2. Sensitivity of Tidal Residual Currents to Stratification Influences on Friction

In this subsection, we briefly examine the sensitivity of the tidally rectified flow component to stratification influences on the vertical eddy viscosity. Note that in the base solutions presented above, the eddy viscosity depends on the local gradient Richardson number via the relationship proposed by *Munk and Anderson* [1948] (see equations (7) - (9) of NLL94). Here we consider nonlinear solutions for the tidally rectified flow component alone with alternative eddy viscosities: those taken from the base solutions and viscosities recomputed without stratification influences included.

The stratification influences on the vertical eddy viscosity do not lead to major qualitative changes in the tidally rectified circulation, but do lead to some significant quantitative ones in the around-bank flow component, e.g., the anticyclonic gyre over Browns Bank. With the stratification-dependent viscosity, we find an enhancement in the around-bank current as stratification evolves from the weakly (winter) to strongly (summer) stratified periods, particularly on Browns Bank.

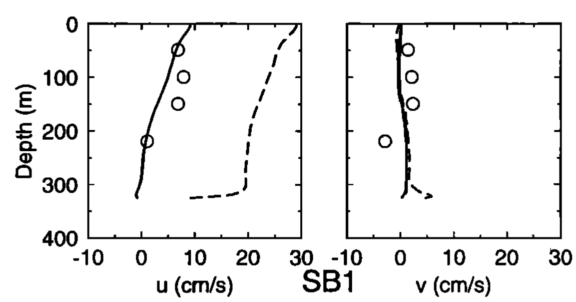


**Figure 10.** Comparison of current profiles from two model solutions with observed bimonthly mean currents (open circles) at site SB1 in the summer season. Here $u$ and $v$ are the eastward and northward components, respectively. Solid lines represent the base case (60-day correlation scale), and dashed lines represent the sensitivity case (30-day scale).

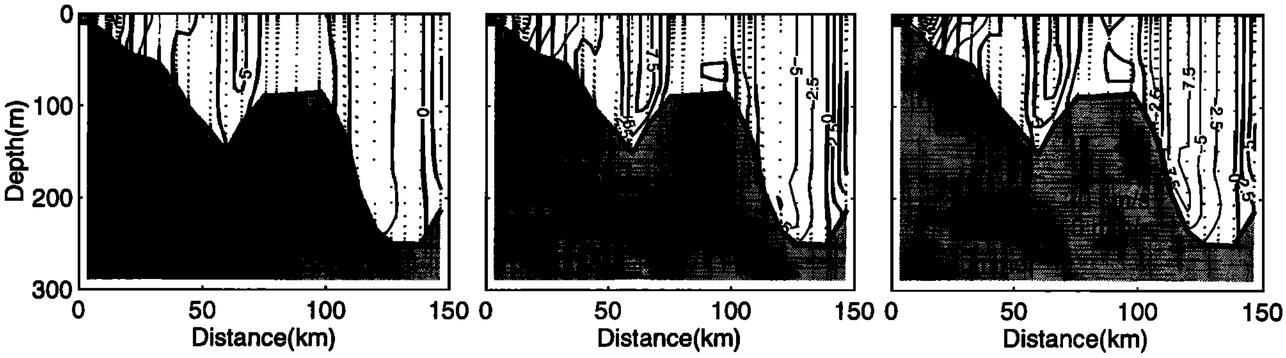


**Figure 11.** Tidal residual velocity on the ESWNS section showing isotachs (centimeters per second) of the normal component (positive into the page) and vectors of the tangential component, with (a) stratification-independent eddy viscosity, (b) stratification-dependent eddy viscosity in winter, and (c) stratification-dependent eddy viscosity in summer. The isotach interval is 2.5 cm/s, with positive (and zero) isotachs in thick lines and negative ones in thin lines.

This increase is illustrated by comparison of the tidally rectified velocity field on the ESWNS section in the different solutions (Figure 11). The stratification influences increase the currents in both winter and summer, with a slightly greater increase in summer. The recirculating transports around Browns Bank are 0.17, 0.19, and 0.20 Sv for the stratification-independent case, winter, and summer, respectively. The above results are qualitatively consistent with previous studies for Georges Bank [*Loder and Wright*, 1985; *Chen*, 1992] (NLL94).

Because of the significant frictional sensitivity of tidal rectification, models with more advanced turbulence closure [e.g., *Lynch et al.*, 1996; *Naimie*, 1996] are desirable for further examination of the circulation on the southwestern Scotian Shelf.

## 5. Summary

The bimonthly flow fields for the winter, spring, and summer seasons presented in section 3 provide a quantitative representation of the three-dimensional seasonal-mean circulation on the Scotian Shelf. Generally, the model results support the conventional understanding that circulation over the Scotian Shelf is dominated by the seasonally varying southwestward flow of relatively cool and fresh shelf water from the Gulf of St. Lawrence and Newfoundland Shelf. The baroclinic pressure field is the predominant forcing of seasonal-mean circulation over the entire shelf. Tidal rectification and wind stress also contribute significantly, particularly on the southwestern Scotian Shelf. Strong tendencies for anticyclonic baroclinic circulation over banks and cyclonic baroclinic circulation over basins are indicated. Connections between the southern Newfoundland and Scotian Shelves vary seasonally, with the present solutions indicating year-round flow along the shelf break. Transport of water from the Gulf of St. Lawrence onto the Scotian Shelf occurs year-round but with variable strength. Further downstream, the cyclonic flow around Emerald Basin plays an important role in connecting the eastern and western Scotian Shelves, while there appears to be a partial bottleneck (and associated offshore turning) of the along-shelf flow off southwestern Nova Scotia (also see *Hannah et al.* [1996]).

Observations of the seasonal-mean circulation are sparse. On the whole, the model solutions compare favorably with the current measurements and transport estimates, indicating that the primary seasonal processes are represented in the model. However, there are significant discrepancies, particularly in the comparison with moored current measurements which shows best agreement in winter and least agreement in spring. The origin of these discrepancies is unclear but in view of the known temporal variability of the Scotian Shelf regime [e.g., *Smith et al.*, 1978; *Smith and Schwing*, 1991], it seems likely that poor observational estimates of the seasonal-mean density and current fields in some areas are a major factor. While the present current data set and model comparisons are not adequate to rule out a significant barotropic inflow across the upstream model boundaries, there is no suggestion in these results that such inflow is a major factor to circulation on the Scotian Shelf away from the shelf break. However, a contribution of upstream barotropic inflow to circulation over the upper continental slope is quite possible (also see *Loder et al.* [1996]).

The present solutions also support the conclusions of *Hannah et al.* [1996] and *Loder et al.* [1996] that in spite of local current discrepancies and marginal density data coverage in some areas, the overall baroclinic circulation patterns on the shelf are generally robust and indicate that baroclinic circulation is the predominant component of seasonal-mean circulation in the region. However, there are significant sensitivities to both data coverage and model parameterizations. In particular, the present solutions point to significant sensitivity of the summer baroclinic circulation at the shelf break on the western Scotian Shelf to the density field estimation procedure. These limitations illustrate the ongoing needs for enhancement of the observational database and more sophisticated (e.g., prognostic) circulation models.

**Acknowledgments.** We are grateful to the many individuals who have contributed to the historical hydrographic database, the FUNDY5IT circulation model, and our analyses. We extend special thanks to Ken Drinkwater and Roger Pettipas for their role in the database assembly, Ross Hendry for providing advice related to the optimal interpolation program, Mary Jo Graça for computing the density fields, Dan Lynch and Chris Naimie for providing the model and advice on its implementation, Dave Greenberg for advice on generating the model grid, and Brian Petrie for providing the Halifax section transport estimates. Helpful comments were received from two JGR reviewers. This work has been jointly funded by the Interim Funding Research Program of the Ocean Production Enhancement Network and the (Canadian) Federal Panel on Energy, Research and Development.

## References

Anderson, C., and P.C. Smith, Oceanographic observations on the Scotian Shelf during CASP, *Atmos. Ocean, 27*, 130-156, 1989.

Bretherton, F.P., R.E. Davis, and C.B. Fandry, A technique for objective analysis and design of oceanographic experiments applied to MODE-73, *Deep Sea Res., 23*, 559-582, 1976.

Brown, W.S., and R.C. Beardsley, Winter circulation in the western Gulf of Maine, 1, Cooling and water mass formation, *J. Phys. Oceanogr., 8*, 265-277, 1978.

Chen, C., Variability of currents in Great South Channel and over Georges Bank: Observation and modelling, Ph.D. dissertation, 283 pp., Woods Hole Oceanogr. Inst., Woods Hole, Mass., June 1992.

Csanady, G.T., The pressure field along the western margin of the North Atlantic, *J. Geophys. Res., 84*, 4905-4915, 1979.

Csanady, G.T., and P. Hamilton, Circulation of slope water, *Cont. Shelf Res., 8*, 565-624, 1988.

de Margerie, S., and K.D. Lank, Tidal circulation of the Scotian Shelf and Grand Bank, Contract report to the Dep. of Fish. and Oceans Can., contract 08SC. FD901-5-X515, Dartmouth, N.S., 1986.

Drinkwater, K.F., B. Petrie, and W.H. Sutcliffe, Seasonal geostrophic volume transport along the Scotian Shelf, *Estuarine Coastal Mar. Sci., 9*, 17-27, 1979.

Drinkwater, K.F., R.A. Myers, R.G. Pettipas, and T.L. Wright, Climatic data for the northwest Atlantic: The position of the shelf/slope front and the northern boundary of the Gulf Stream between 50°W and 75°W, 1973-1992, *Can. Data Rep. Fish. Ocean Sci., 125*, 107pp., 1994.

El Sabh, M.I., Oceanographic features, currents and transport in Cabot Strait, *J. Fish. Res. Board Can., 34*, 516-528, 1977.

Greenberg, D.A., Modeling the mean barotropic circulation in the Bay of Fundy and the Gulf of Maine, *J. Phys. Oceanogr., 13*, 886-904, 1983.

Gregory, D., and P.C. Smith, Current statistics of the Scotian Shelf and Slope, *Can. Tech. Rep. Hydrography and Ocean Sci., 106*, 197pp., 1988.

Han, G., M. Ikeda, and P.C. Smith, Annual variation of sea-surface slopes over the Scotian Shelf and Grand Banks from Geosat altimetry, *Atmos. Ocean, 31*, 591-615, 1993.

Han, G., M. Ikeda and P.C. Smith, Oceanic tides over the Scotian and Newfoundland Shelves from TOPEX/POSEIDON altimetry, *Atmos. Ocean*, in press, 1996.

Hannah, C.G, J.W. Loder, and D.G. Wright, Seasonal variation of the baroclinic circulation in the Scotia-Maine region, in *Bouyancy Effects on Coastal Dynamics, Coastal Esturine Stud.*, Vol. 53, edited by D.G. Aubrey and C.T. Friedrichs, AGU, Washington, D.C., in press, 1996.

Loder, J.W., and D.G. Wright, Tidal rectification and frontal circulation on the sides of Georges Bank, *J. Mar. Res., 43*, 581-604, 1985.

Loder, J.W., G. Han, C.G., Hannah, D.A. Greenberg, and P.C. Smith, Hydrography and baroclinic circulation in the Scotian Shelf region: Winter vs. summer, *Can. J. Fish. Aquat. Sci., suppl.*, in press, 1996.

Lynch, D.R., and C.E. Naimie, The $M_2$ tide and its residual on the outer banks of the Gulf of Maine, *J. Phys. Oceanogr. 23*, 2222-2253, 1993.

Lynch, D.R., F.E. Werner, D.A. Greenberg, and J.W. Loder, Diagnostic model for baroclinic, wind-driven and tidal circulation in shallow seas, *Cont. Shelf Res., 12*, 37-64, 1992.

Lynch, D.R., J.T.C. Ip, C.E. Naimie, and F.E. Werner, Comprehensive coastal circulation model with application to the Gulf of Maine, *Cont. Shelf Res., 16*, 875-906, 1996.

McLellan, H.J., Temperature-salinity relations and mixing on the Scotian Shelf, *J. Fish. Res. Board Can., 11*, 419-430, 1954.

Munk, W.H., and E.R. Anderson, Notes on a theory of the thermocline, *J. Mar. Res., 7*, 276-285, 1948.

Naimie, C.E., Georges Bank residual circulation during weak and strong stratification periods: Prognostic numerical model results, *J. Geophys. Res., 101*, 6469-6486, 1996.

Naimie, C.E., and D.R. Lynch, *FUNDY5 Users' Manual*, Numer. Meth. Lab., 40pp., Dartmouth College, Hanover, N.H., 1993.

Naimie, C.E., J.W. Loder, and D.R. Lynch, Seasonal variation of the three-dimensional residual circulation on Georges Bank, *J. Geophys. Res., 99*, 15,967-15,989, 1994.

Ramp, S.R., J. Schlitz, and W.R. Wright, The deep flow through the Northeast Channel, Gulf of Maine, *J. Phys. Oceanogr., 15*, 1790-1808, 1985.

Schwing, F.B., Subtidal response of Scotian Shelf circulation to local and remote forcing, 1, Observations, *J. Phys. Oceanogr., 22*, 523-541, 1992a.

Schwing, F.B., Subtidal response of Scotian Shelf circulation to local and remote forcing, 2, Barotropic model, *J. Phys. Oceanogr., 22*, 542-563, 1992b.

Sheng, J., and K.R. Thompson, A robust method for diagnosing regional shelf circulation from scattered density profiles, *J. Geophys. Res., 101*, 25,647-25,659, 1996.

Smith, P.C., The mean and seasonal circulation of southwest Nova Scotia, *J. Phys. Oceanogr., 13*, 1034-1054, 1983.

Smith, P.C., The distribution of surface wind over the Scotian Shelf, in *Proceedings of the International Workshop on Wave Hindcasting and Forecasting, Rep. Ser. 065*, pp., 25-36, Environ. Stud. Revolving Fund, Ottawa, 1987.

Smith, P.C., Seasonal and interannual variability of current, temperature and salinity off southwest Nova Scotia, Can. *J. Fish. Aquat. Sci., 46*, 4-20, 1989.

Smith, P.C., and B. Petrie, Low-frequency circulation at the edge of the Scotian Shelf, *J. Phys. Oceanogr., 12*, 28-46, 1982.

Smith, P.C., and F.B. Schwing, Mean circulation and variability on the eastern Canadian continental shelf, *Cont. Shelf Res., 11*, 977-1012, 1991.

Smith, P.C., B. Petrie, and C.R. Mann, Circulation, variability and dynamics of the Scotian Shelf and Slope, *J. Fish. Res. Board Can.*, *35*, 1067-1083, 1978.

Smith, S.D., Coefficients for sea surface wind stress, heat flux, and wind profiles as a function of wind speed and temperature, *J. Geophys. Res.*, *93*, 15,467-15,472, 1988.

Sutcliffe W.H., R.H. Loucks, and K.F. Drinkwater, Coastal circulation and physical oceanography of the Scotian Shelf and Gulf of Maine, *J. Fish. Res. Board Can.*, *33*, 98-115, 1976.

Tee, K.T., P.C. Smith, and D. LeFaivre, Topographic upwelling off southwest Nova Scotia, *J. Phys. Oceanogr.*, *23*, 1703-1726, 1993.

Trites, R.W., and R.E. Banks, Circulation on the Scotian Shelf as indicated by drift bottles, *J. Fish. Res. Board Can.*, *15*, 79-89, 1958.

Wright, D.G., D.A. Greenberg, J.W. Loder, and P.C. Smith, The steady-state response of the Gulf of Maine and adjacent regions to surface wind stress, *J. Phys. Oceanogr.*, *16*, 947-966, 1986.

G. Han, J. W. Loder, and P. C. Smith, Fisheries and Oceans Canada, Bedford Institute of Oceanography, P.O. Box 1006, Dartmouth, Nova Scotia, Canada B2Y 4A2.

C. G. Hannah, Oceadyne Environmental Consultants, 373 Ridgevale Drive, Bedford, Nova Scotia, Canada B4A 3M2.

(Received April 3, 1996; revised September 13, 1996; accepted October 3, 1996.)